Available online at www.sciencedirect.com
ScienceDirect
Journal of Molecular Catalysis A: Chemical 281 (2008) 192–199
JOURNAL OF MOLECULAR CATALYSIS A: CHEMICAL
www.elsevier.com/locate/molcata

Antibacterial activity of montmorillonites modified with silver

S.M. Magaña [a], P. Quintana [a,*], D.H. Aguilar [a], J.A. Toledo [b], C. Ángeles-Chávez [b], M.A. Cortés [b], L. León [a], Y. Freile-Pelegrín [a], T. López [c,d], R.M. Torres Sánchez [e]

[a] *CINVESTAV-Mérida, Depto. de Física Aplicada y Depto. de Recursos del Mar, A.P. 73, Cordemex, Mérida, Yuc. México C.P. 97110, Mexico*
[b] *Instituto Mexicano del Petróleo, Av. Lázaro Cardenas # 152, México, D.F., Mexico*
[c] *Nanotechnology Materials Laboratory, Universidad Autónoma Metropolitana -Rectoría General, Prol. Canal de Miramontes 3855, Col. Ex-Had. San Juan de Dios, Tlalpan 14387, México, D.F., Mexico*
[d] *Instituto Nacional de Neurología y Neurocirugía "Manuel Velasco Suárez", Av. Insurgentes Sur # 3877, México C.P. 14269, D.F., Mexico*
[e] *CONICET-CETMIC, Camino Centenario y 506 (B1897ZCA) M.B. Gonnet, Argentina*

Available online 30 October 2007

Abstract

The antibacterial properties of silver modified montmorillonites from Pellegrini Lake, Argentina were tested in growth inhibition of *Escherichia coli* bacteria. Montmorillonite was first submitted to different treatments: (a) calcination at 550 °C for 3 h and (b) grinding during 300 s. After that, the samples were loaded with silver by ion exchange. Structural characterization was performed by X-ray diffraction (XRD), Fourier transformed infrared spectroscopy (FTIR), and BET specific surface area measurements. Scanning electron microscopy (SEM) and high resolution transmission electron microscopy (HRTM) showed that metallic silver nanoparticles precipitates over the clay surface after silver modification. Nevertheless, the displacement of the (0 0 1) reflection observed by XRD in the calcined sample, and the diminution in Na^+ content evaluated by energy dispersive X-ray spectroscopy (EDXS), indicate that Ag ions were interchanged in the structure of the clays. Both samples showed good antibacterial activity against *E. coli*, measured by the disk susceptibility and the minimum inhibitory concentration (MIC) tests. The ground montmorillonite required a lower MIC than the thermally treated, although the last one presented a bigger inhibition zone in the disk method. The results shows that the antibacterial activity is generated by the Ag^+ present in the clay, as confirmed by X-ray photoelectronic spectroscopy (XPS); however the overall antibacterial properties are affected by the availability of the ionic silver to be in contact with the bacteria.

Keywords: Montmorillonite; Antibacterial activity; Silver; X-ray diffraction; FTIR; BET; HRTEM; EDXS; XPS; Disk susceptibility test; MIC

1. Introduction

The development of materials with the ability to inhibit bacterial growth have been of great interest in recent years due to their potential use in everyday products like paints, kitchenware, school and hospital utensils, etc. Inorganic antibacterial materials have several advantages over traditionally used organic agents; like chemical stability, thermal resistance, safety to the user, long lasting action period, etc. [1].

Antibacterial inorganic materials are generally based in metallic ions with antibacterial properties, like Ag^+ or Cu^{2+}, which are loaded into a ceramic matrix by ion exchange. Clays [2,3], zeolites [4,5] and other aluminosilicates [1,6] have been used as carriers with good results because their high ion exchange capacity, high surface area and sorptive capacity, negative surface charge, chemical inertness and low or null toxicity [7].

Smectites, classified as 2:1 phyllosilicate clays, have a unit crystal lattice formed by one alumina octahedral sheet sandwiched between two silica tetrahedral sheets; the interlayer between units contain positive cations and water molecules. Due to this crystalline arrangement, smectites are able to expand and contract the interlayer while maintaining two-dimensional crystallographic integrity; and are characterized by octahedral and/or tetrahedral substitution and high ion-exchange capacities (70–120 mequiv./100 g). Montmorillonite and beidellite are some of the members of the smectite family [8,9].

It have been shown that metallic ion-exchanged montmorillonite dispersed in water attracts and adsorbs negatively charged

* Corresponding author. Tel.: +52 9991242142; fax: +52 9999812917.
E-mail address: pquint@mda.cinvestav.mx (P. Quintana).

1381-1169/$ – see front matter © 2007 Elsevier B.V. All rights reserved.
doi:10.1016/j.molcata.2007.10.024

bacteria, improving the antibacterial properties of the material [10]; also is a good adsorbent for charged or non-charged organic molecules like aflatoxins, salicylic acid, herbicides and fungicides [11–15].

Clay properties as surface area and cation exchange capacity can be modified through several methods like thermal treatment or mechanical grinding; for example, adsorption capacity of bentonite was enhanced after calcination of the mineral [16,17]. The main effects of these treatments are the collapse of the interlayer and the introduction of structural alterations, diminishing the swelling capacity of the raw clay and modifying the surface charge, respectively [18]. For example, the point of zero charge (PZC) of the calcined or mechanical ground montmorillonite, increases up to pH 8.0, due to the release of structural Al^{3+} which produce an edge enrichment with aluminum ions or oligomeric hydroxoaluminium cations [15,18].

In this work, we report the antibacterial activity of silver exchanged montorillonite from Pellegrini Lake, Argentina. The clay was submitted to different treatments: (a) calcination at 550 °C for 3 h and (b) grinding during 300 s; and then ion exchanged with silver. Antibacterial activity was evaluated through growth inhibition of *Escherichia coli* measured by the disk susceptibility test. The minimum inhibitory concentration (MIC) for antibacterial activity was determined by the agar dilution method.

2. Experimental

2.1. Preparation of Ag-exchanged montmorillonites

Montmorillonite clay minerals, <5 μm-montmorillonite (99% purity), were isolated by dispersion in water and further centrifugation (Sharples continuous ultracentrifuge) at 10,000 rpm, from a bentonite sample collected from Lago Pellegrini deposit (Rio Negro, North Patagonia; Argentine); the montmorillonite percentage recovered after the centrifugation was around 82% [19]. The obtained montmorillonite, designed as B-N, was subjected to different treatments: (a) calcination at 550 °C for 3 h (labeled B-550T) and (b) mechanical grinding, during periods of 100 s with stops to avoid heating of the milling chamber and the sample (labeled B-300S). A Herzog HSM 100 oscillating mill was used, with a hollow Cr-steel cylinder milling chamber and milling tools consisting of a ring and a solid cylinder of the same material. The sample was distributed in the free space between these pieces. The point of zero charge (PZC) was pH 3.9, 8.3 and 8.0 for B-N, B-550T, and B-300S, respectively [20].

Silver loading was carried out only in the treated clays, labeled B-550T/Ag, and B-300S/Ag; by mixing 30 mL of $AgNO_3$ 0.1N with 3 g of each sample to obtain a 30% (w/w) suspension, and maintained with a continuous stirring during 1 week. After this equilibration time, the samples were washed with distilled water by centrifugation (3500 rpm during 30 min) until no Ag^+ was determined in the supernatant solution (AgCl test). Precautions were taken for the light sensitivity of silver.

2.2. Characterization

2.2.1. X-ray diffraction (XRD)

Structural characterization was carried out by X-ray diffraction in a Siemens D-5000 diffractometer operated at 35 kV and 25 mA, with Cu Kα radiation (λ = 1.5418 Å). The powdered samples, maintained at room humidity (43% relative humidity), were registered with a step time of 10 s and a step size of 0.02°, for a total registering time of 13 h. The clays were analyzed before and after the silver loading to evaluate any possible structural change.

2.2.2. Fourier transformed infrared spectroscopy (FTIR)

The natural and treated clays were analyzed on a Thermo Nicolet Nexus 670 FTIR spectrometer, equipped with a deuterated triglycine sulfate (DTGS) KBr detector and purge gas generator. Samples were recorded at a spectral resolution and wavenumber precision of 0.09 and 0.01 cm^{-1}, respectively. The powdered clays (5.0 mg) were mixed thoroughly in agate mortar with KBr (195 mg) until homogenization, placed into the Smart Multi-Bounce HATR sample compartment of the spectrometer and continuously purged with dry air. For each spectrum, 64 scans were acquired at a spectra resolution of 4 cm^{-1}.

2.2.3. Surface area and pore distribution measurements

Specific surface area was measured with a micromeritics (ASAP 2010) equipment degasifying the samples at 50 °C. Surface area was calculated from the nitrogen isotherms using the Brunauer–Emmet–Teller (BET) equation. The mean pore diameter was obtained by applying the Barret–Joyner–Halenda (BJH) method.

2.2.4. Electron microscopy and energy dispersive X-ray spectroscopy (EDXS)

Scanning electron microscopy (SEM) and chemical analysis by EDXS were performed in an environmental scanning electron microscope XL30, which has attached an energy dispersive X-ray spectroscope. High angle annular dark field scanning transmission electron microscopy (HAADF-STEM) and high resolution transmission electron microscopy (HRTEM) analysis of the samples were performed in a JEM-2200FS transmission electron microscope with accelerating voltage of 200 kV. The microscope was equipped with a Schottky-type field emission gun and ultra high resolution (UHR) configuration (Cs = 0.5 mm, Cc = 1.1 mm, point to point resolution = 0.19 nm) and in-column omega-type energy filter. Local chemical analysis by energy dispersive X-ray spectrometry (EDXS) was performed in a NORAN energy dispersive X-ray spectroscope, which is attached to the microscope using the STEM-EDX combination. The samples were ground, suspended in isopropanol at room temperature, and dispersed with ultrasonic agitation; then, an aliquot of the solution was dropped on a 3 mm diameter lacey carbon copper grid.

2.2.5. X-ray photoelectronic spectroscopy (XPS)

XPS spectra were recorded on a Thermo-VG Scalab 250 spectrometer equipped with Al Kα X-ray source (1486.6 eV)

and a hemispherical analyzer. The base pressure during the analysis was 10^{-9} Torr. The Ag $3d_{5/2}$ experimental peak was deconvoluted through the XPS peak fit software, using mixed Gaussian–Lorentzian functions, non-linear squares fitting algorithm and Shirley-type background subtraction. The binding energies (BE) were referenced to the adventitious carbon C 1s peak at 284.6 eV. Changes in the Ag $3d_{5/2}$ signal shape on the samples were analyzed by a curve fitting procedure with doublets endowed with fixed spectroscopic parameters, but using variable position, full width at half maximum (FWHM) and intensities. The surface composition was determined from the corresponding peak areas after subtracting the inelastic background and correction of the peak areas by the respective sensitive factors provided by the manufacturer of the XPS apparatus.

2.3. Evaluation of antibacterial activity

2.3.1. Disk susceptibility test

Antibacterial activity of the Ag exchanged clays was tested on *E. coli* (ATCC 25922 Benton Dickinson Microbiology Systems) by the disk susceptibility test [21]. The bacteria was cultured on Mueller–Hinton agar at 37 °C during 24 h; three to five colonies were diluted in Mueller–Hinton broth and the suspension was adjusted to 0.5 McFarland turbidity (1.5×10^8 CFU). A sterile cotton swab was used to inoculate the surface of another Mueller–Hinton agar plate, rotating the plate every 60° to ensure homogeneous growth. The natural and treated samples (50 mg), with and without silver, were pressed into pellets (7 mm diameter) and placed over the surface of the agar plates. The width of inhibition was measured after 24 h of incubation at 37 °C. Ampiciline/Sulbactam was used as a standard for antibacterial susceptibility.

2.3.2. Minimum inhibitory concentration (MIC)

Minimum inhibitory concentration of the treated montmorillonites was determined by the agar dilution method [22]. Montmorillonite powders were dried in an oven at 50 °C for 2 h, weighted (20, 10, 5, 2.5, 2, 1 and 0.5 mg) in an analytical balance, and exposed to UV radiation during 30 min to ensure sterilization. After that, the powders were added to an agar suspension at 50 °C, transferred to a cell and slowly cooled until the formation of a gel. Since agar gelation is produced exclusively by formation of hydrogen bonds, no interference is expected from the presence of the clays in the gelation process; only agents which strongly capture protons, like urea, guanidine, sodium thiocyanate or potassium iodide can block agar gelation by avoiding the formation of hydrogen bridges [23]. The agar cells were inoculated with 50 μL of bacterial culture, adjusted up to 0.5 McFarland turbidity and incubated at 37 °C for 24 h.

3. Results

3.1. Characterization

The X-ray diffraction pattern (Fig. 1) of the natural clay was identified as a montmorillonite, $Na_{0.3}Al_2(Si,Al)_4O_{10}(OH)_2{\cdot}2H_2O$, with a (0 0 1) interlayer spacing of 12.41 Å

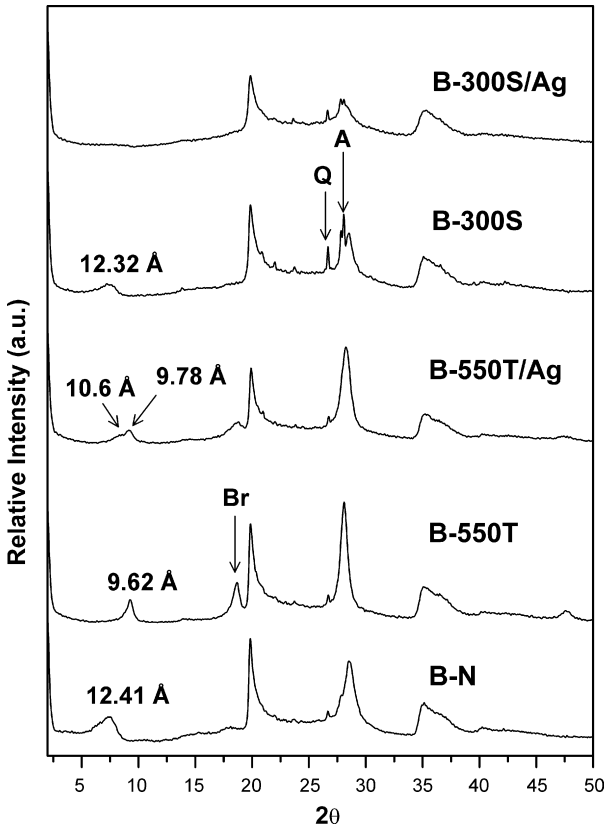

Fig. 1. X-ray patterns of the natural (B-N); calcined (B-550T) and mechanically ground (B-300S) clays. Ag indicates the samples after silver cation exchange. Br = brammallite, Q = quartz and A = anorthite.

(7.129° 2θ) [20,24]. Small quantities of quartz, at 26.68° (2θ), and anorthite, at 21.95°, 23.65°, 27.77° and 28.12° (2θ), were also observed. For the calcined sample (B-550T) the powder pattern changed. The (0 0 1) peak became narrower, its intensity increases, and the position shifts to a lower d-spacing, 9.62 Å (9.2° 2θ); and a new reflection appears at 4.76 Å (18.6° 2θ). This implies a structural change to brammallite, $NaAl_2(Si,Al)_4O_{10}(OH)_2$, due to the loss of water present in the interlayer [25–27].

In the milled sample, B-300S, the (0 0 1) peak almost disappear, and the position slightly shifts to 12.32 Å (7.17° 2θ). The diminution on the intensity and the displacement of the peak indicates that the long range interlayer structure along the *c*-axis was damaged by grinding [16,28,29]. Quartz and anorthite peak intensity increases because grinding breaks up the clay particles, promoting the separation of the mineral phases. There is no reported antibacterial activity by these minerals, so no interference is expected in the antibacterial test.

After ion-exchange, the diffractograms showed some differences. The peak at 4.76 Å (18.6° 2θ) in B-550T/Ag, became broader and less intense; whereas the (0 0 1) reflection moves to a higher *d*-spacing value due to the reintroduction of water in the interlayer. It has been reported that the amount of water adsorbed by smectites is affected by the interlayer ion identity, charge sites and electrostatic forces of attraction between the positively charged interlayer cation and the negatively charged 2:1 phyllosilicate layer [30,31].

From Fig. 1 it can be seen that in B-550T/Ag the (0 0 1) peak presents two components at 10.6 Å (8.34° 2θ) and 9.78 Å (9.08° 2θ), positioned in-between the natural (12.41 Å) and calcined (9.62 Å) samples. The *d*-spacing position and shape differences of the (0 0 1) reflection suggest the introduction of Ag^+ ions within the structural interlayer.

On the other hand, the (0 0 1) reflection in B-300S/Ag disappeared, indicating the complete collapse of the interlayer; which was attributed by Sondi et al. [28] to cleaveage along the basal plane of the clay particles. In this case, silver ions can be incorporated in the clay by surface and edge reactive sites, which preferably bind charged species and can average up to a 20% of the total cation exchange capacity (CEC) [31]. Metallic silver was not detected in the interchanged samples, which is in concordance with other works [1,5].

FTIR of the clay samples before Ag modification showed the typical absorption bands of aluminosilicates (Fig. 2). In the high frequency range a well-defined peak appears at 3625 cm^{-1}, associated to the stretching mode of the OH-group coordinated to Al cations [12,20]. Kloprogge et al. [32], proposed that the wide band between 3000 and 3500 cm^{-1} is composed at least by three different bands: H_2O–H_2O–H bonds that absorbs around 3398 cm^{-1}; a band at 3200 cm^{-1} ascribed to an overtone of the H_2O bending vibration; and an absorption below 3200 cm^{-1} due to the presence of small and strongly polarizing cations, such as Al^{3+}, since H_2O molecules coordinated to them form stronger H bonds to H_2O in outer spheres of coordination. The bands observed at 1625 and 1697 cm^{-1} are related to H_2O bending mode, the presence of two bands indicate differences in coordination water within the structure and the hydration shell.

For the treated clays, no changes are observed for structural hydroxyls (3625 cm^{-1}); however, the stretching band related to water–OH bond (3398 cm^{-1}), decreases in the calcined sample (B-550T) due to water loss; and increases in the milled one since grinding modifies the particle size and favors water adsorption. The major difference was observed for the water-OH bending mode, (1625 and 1697 cm^{-1}) which almost disappears with heating. On the other hand, after the grinding treatment, the band at 1625 cm^{-1} strongly increases, whereas the absorption at 1695 cm^{-1} diminishes; this implies a change in coordinated water, possibly in the clay structural interlayer, since XRD showed that the samples became less crystalline after grinding.

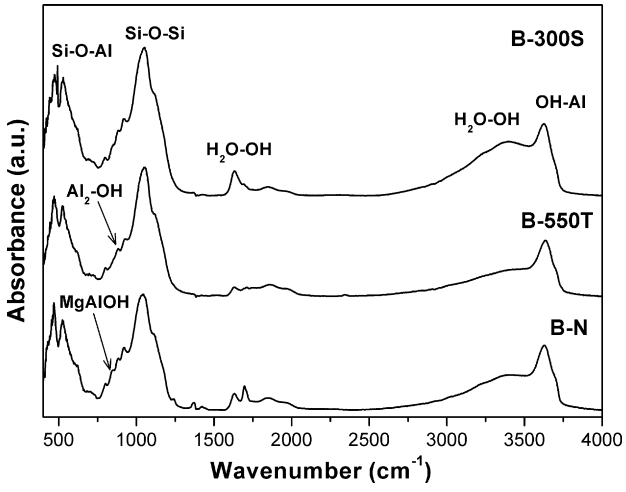

Fig. 2. Infrared spectra for natural clay (B-N), and after calcination (B-550T) and grinding (B-300S).

Table 1
Elemental analysis (wt%) of natural montmorillonite (B-N), calcined (B-550T) and ground (B-300S) clays, and the corresponding samples exchanged with silver (B-500T/Ag and B-300S/Ag)

Element	B-N	B-550T	B-550T/Ag	B-300S	B-300S/Ag
Si	34.68	36.03	35.22	34.02	32.20
Al	12.60	12.89	13.00	12.17	11.65
Fe	8.49	5.8	5.56	5.66	4.73
Mg	2.61	2.69	2.78	2.55	2.28
Na	1.72	1.79	1.31	1.92	0.78
Ca	0.5	0.42	0.21	0.52	–
K	–	0.32	–	0.36	–
Cl	–	–	–	0.23	–
F	–	–	1.05	–	–
O	39.4	40.04	37.51	42.56	39.99
Ag	–	–	3.36	–	8.37
% Total	100	100	100	100	100

In the lower frequency range (750–1300 cm^{-1}), the most intense band at 1045 cm^{-1} and a shoulder at 1108 cm^{-1} are related to stretching Si–O–Si bond, characteristic of phyllosilicate minerals [33]. The lower wavenumber belongs to the Si–O outside plane, the higher one is associated to in-plane vibrations [16]. MgAlOH and Al_2–OH deformations are observed at 848 and 921 cm^{-1}; whereas the two strong bands at 450 and 550 cm^{-1} corresponds to the bending mode of Si–O and Si–O–M bonds (where M = Mg, Al and Fe), respectively [32].

The montmorillonite characteristic bands for Si–O–Si bonding (1045 and 1108 cm^{-1}) remain the same after the treatment for B-550T and B-300S samples. On the other hand, the MgAlOH bending band (848 cm^{-1}) became very small, this difference could be related to the migration of Al and Mg ions to the surface [25]. When clays were exchanged with silver, no modifications were observed on the infrared spectra.

Elemental chemical analysis by EDXS was carried out in all the samples (Table 1). After the ionic exchange, total Ag content was 3.36 wt% for the calcined clay and 8.37 wt% for the ground sample. Carbon was not detected. Both silver treated samples showed a diminution of Na^+, K^+ and Ca^{2+} content after ion exchange; the decrement was stronger in the ground sample. It have been reported that Na^+ is preferentially exchangeable by Ag^+, therefore, the decrease in sodium content can be associated with the incorporation of Ag^+ ions in the samples by cation exchange [5,34].

From SEM images (Fig. 3) it was observed that the treated clays (B-550T and B-300S) are composed of heterogeneous particles. The heated sample presented a layered flake morphology characteristic of clays, with particle size between 5 and 50 μm (Fig. 3a); whereas the ground one, was composed of agglomerates with a rough shape and a smaller particle size between 1 and 20 μm (Fig. 3b). After Ag modification, HAADF-STEM images showed the presence of white nanoparticles on the surface of the exchanged samples, which are below 10 nm (Fig. 3c)

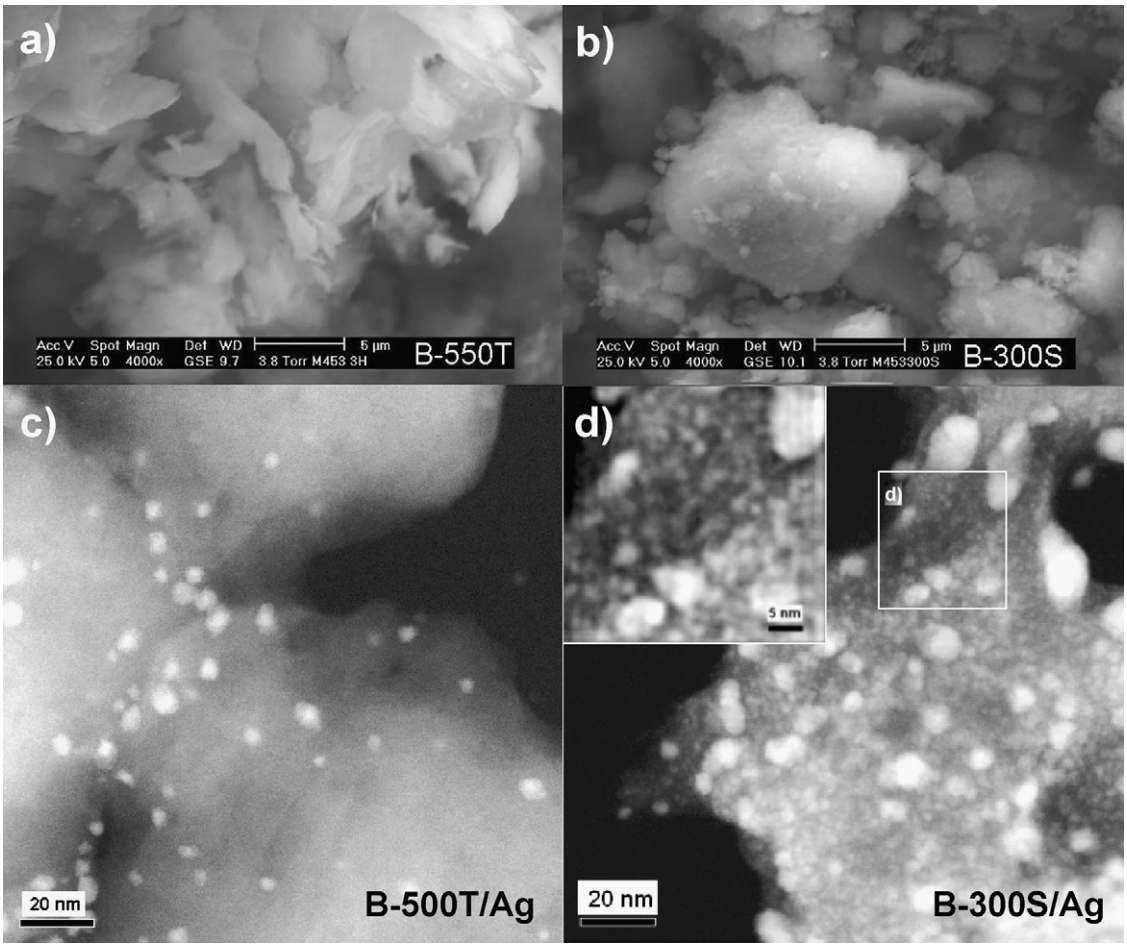

Fig. 3. SEM micrographs of montmorillonites: (a) calcined sample (B-550T), (b) ground sample (B-300S). HAADF-STEM micrographs of silver loaded clays: (c) calcined sample (B-550T/Ag), (d) ground sample (B-300S/Ag). Inset in Fig. 3(d) shows a zone with nanoparticles smaller than 5 nm.

in B-550T/Ag, and have a homogeneous distribution. On the other hand, B-330S/Ag showed a heterogeneous distribution of bigger particles (25–10 nm) along with nanoparticles smaller than 3 nm that are present in the clay surface (Fig. 3d). This smaller nanoparticles were not observed in the calcined sample.

HAADF-STEM provides a significant atomic number dependent contrast (Z contrast) and is quite useful to determine the local chemical structure at atomic scale, therefore, these nanoparticles with white contrast can be associated to the formation of metallic silver. HRTEM was performed over the white nanoparticles (Fig. 4); the analysis of the images showed *d*-spacing distances around 0.238, 0.236 and 0.203 nm, which are similar to the corresponding (−1,−1,1), (1 1 1) and (0 0 2) planes of metallic silver in the (1,−1,0) direction (JC-PDF card No. 4-7803). Local chemical analysis by STEM-EDXS performed in the white nanoparticles (not shown) confirmed that they were rich in Ag atoms, supporting very well the result observed in HAADF-STEM image.

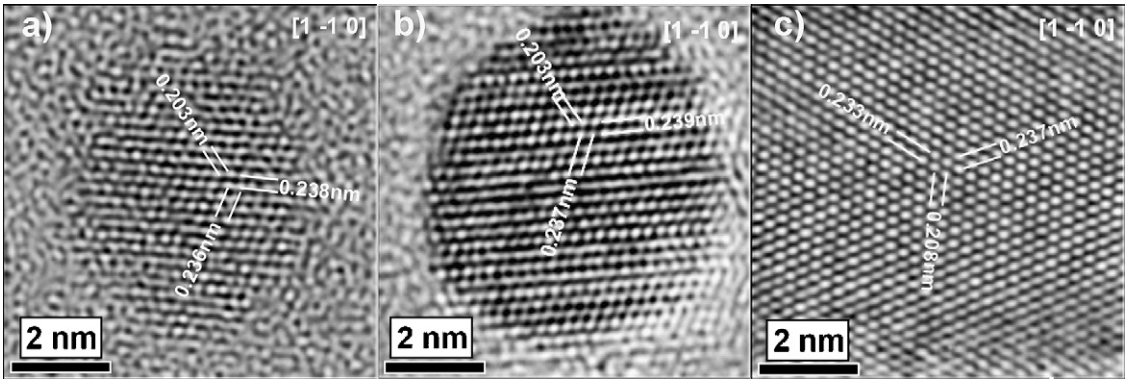

Fig. 4. HRTEM electron diffraction images of silver nanoparticles in the: (a) calcined sample (B-550T/Ag), (b) and (c) ground sample (B-300S/Ag).

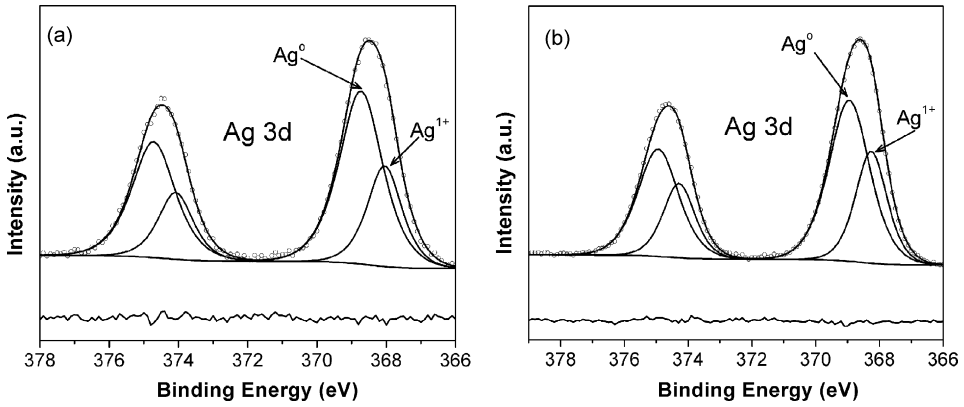

Fig. 5. XPS spectra of the Ag $3d_{5/2}$ region in (a) B-550T/Ag and (b) B-300S/Ag samples.

Table 2
XPS parameters of the Ag ($3d_{5/2}$) region in samples containing Ag

Sample	B.E. Ag $3d_{5/2}$ (FWHM) (eV)	Assignment	Surface concentration (at.%)	Ag^{1+}/Ag^0 atomic ratio
B-550T/Ag	368.0 (1.2)	Ag^{1+}	0.67	0.45
	368.7 (1.5)	Ag^0	1.46	
B-300S/Ag	368.2 (1.2)	Ag^{1+}	1.57	0.54
	368.9 (1.6)	Ag^0	2.93	

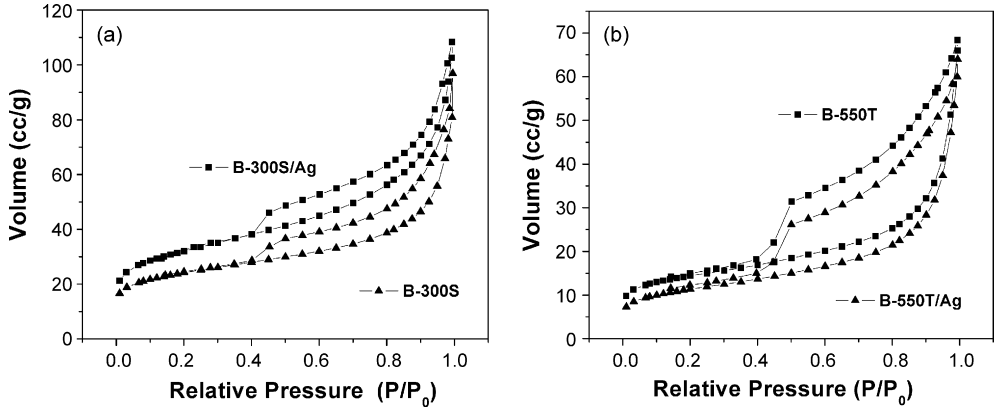

Fig. 6. Adsorption–desorption isotherms of the samples with and without silver: (a) ground clay during 300 s and (b) calcined clay at 550 °C.

There are contradictory reports about the antibacterial properties of metallic silver. Studies carried out by the electrochemical method showed that no antibacterial activity occurs when silver is in the metallic state [35,36]; nevertheless, other works report good antibacterial properties when Ag^+ ions (as Ag_2O or AgOH) are formed on the surface of metallic silver nanoparticles [37,38].

XPS measurements were carried out to detect the oxidation state of silver present in the clay. XPS spectra of the Ag $3d_{5/2}$ peak for B-300S/Ag and B-550T/Ag are shown in Fig. 5. The peaks were fitted by using two doublets with the BE and FHWM values reported in Table 2; BE values were assigned to different Ag oxidation states according to literature data [39]. The silver $3d_{5/2}$ signal at 368.0 ± 0.2 eV, corresponds to Ag^+ ions, whereas that occurring at 368.7 ± 0.2 is related to metallic Ag^0 [40]. The detected Ag^+ signal could be attributed to the formation of Ag_2O or AgOH on the surface of the silver nanoparticles smaller than 5 nm [37]; but also to the presence of silver ions interchanged in the clay in edge or surface sites. A higher superficial silver content was detected in the ground sample; nevertheless, the Ag^+/Ag^0 relationship (Table 2) was only slightly higher in the milled sample than in the calcined one.

Table 3
Surface area, pore volume and pore size values for different clay samples

Sample	Specific surface area (m^2/g)	Pore volume (cm^3/g)	Pore size (Å)
B-N	53.19	0.0871	65.516
B-550T	48.85	0.0943	77.266
B-550T/Ag	38.81	0.0873	86.891
B-300S	82.04	0.1131	57.616
B-300S/Ag	109.53	0.1439	52.554

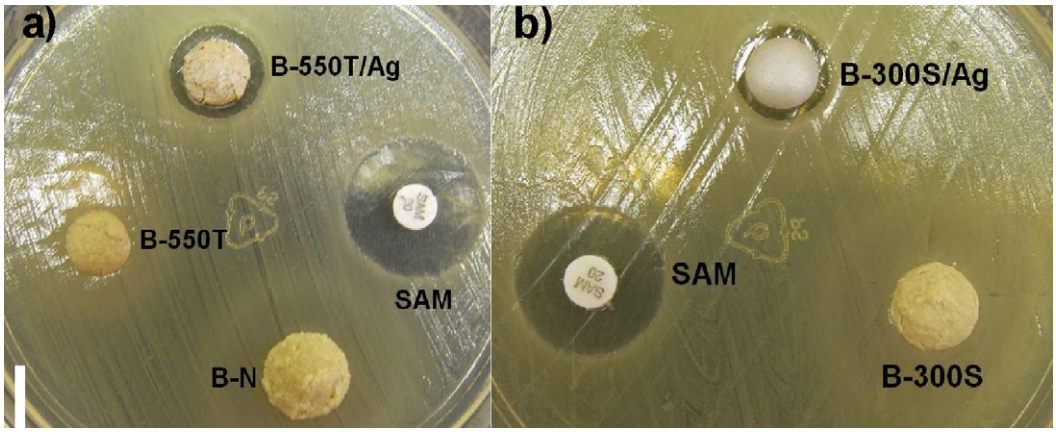

Fig. 7. Comparison of the inhibition zone test between the standard antibacterial material (SAM, Ampicilin/Sulbactam) and natural clay (B-N) with: (a) clay calcined at 550 °C (B-550T) with and without Ag and (b) ground sample (B-300S) with and without Ag.

Experimental gas adsorption isotherms (Fig. 6) correspond to type IV, characterized by a prominent adsorption at low relative pressure, with a hysteresis loop type H4 according to IUPAC [41]. This behavior is typical of an adsorption process on mesoporous solids via multilayer adsorption followed by a capillary condensation [42]. Therefore, initially is similar to that of macroporous solids, but at higher pressures the adsorbed amount rises very steeply due to the capillary condensation in mesopores. After this, pores are filled and the adsorption isotherms levels off. The natural clay isotherm (not shown) presented low porosity on the micro and mesoporous region, with a low pore volume and surface area, which is similar to the calcined sample. However, for the ground clay, this values increases with a diminution on the pore size. After been interchanged with silver, the specific surface area and the pore volume increases for the milled sample, but the pore size diminishes. A contrary effect was observed for B-550T/Ag (Table 3).

The obtained specific surface area of B-N is comparable to pillared clays [43] and Cu–Ca montmorillonite [10] reported elsewhere. Thermal and grinding treatments produce opposite behavior on the specific surface area, slight decrease and a strong increase, respectively, in agreement with the results found by SEM and the reported by Bojemueller et al. [15] and Torres Sanchez et al. [24], whereas, the specific surface area values after silver loading follows the previous behavior.

3.2. Antibacterial activity

The disk susceptibility tests are shown in Fig. 7 and the results are given in Table 4. The inhibition zone diameter and the amount of swelling from the edge of each disk in the agar plate are given in mm. The test was repeated at least three times, for each treated sample. No antibacterial activity was detected.

Table 4
Zone of inhibition test results, all reported data correspond to the mean value

Sample	Initial diameter (mm)	Final inhibition zone diameter (mm)	Diffusion (mm)
B-N	7	12.0	5.0
B-550T	7	9.2	2.2
B-550T/Ag	7	13.3	2.5
B-300S	7	10.7	3.7
B-300S/Ag	7	12.3	2.0

Both silver exchanged samples presented good antibacterial activity, with a mean diameter of 13.3 and 12.3 mm of inhibition zone for B-550T/Ag and B-300S/Ag, respectively. Although, XPS analysis showed that the calcined sample present a lower Ag^+/Ag^0 relationship than the milled one, these results agrees with other works, where higher silver loadings does not lead to a higher antibacterial activity [4,5].

Our results are comparable to the ones reported by Dizman et al. [6] using phyllosillicates as micas or by Top et al. [4] using framework structures as Na-clinoptilolite interchanged with silver and copper; however, Li et al. [1] obtained a higher inhibition zone with vermiculite interchanged with copper.

The minimum inhibitory concentration (MIC) of antimicrobial agents was determined by the lowest concentration agent that completely inhibits visible growth, as judged by the naked eye, disregarding a single colony or a thin haze within the area of the inoculated spot. This test was replicated and the results were the same. The MIC values against *E. coli* of the treated clays were 2.5 and 1 mg for B-550T/Ag and B-300S/Ag, respectively.

The antibacterial properties of silver exchanged montmorillonites have been attributed to the attraction, by electrostatic forces, of the negatively charged membrane of the bacteria to the surface of the clay, where the positive charged silver ions kills the bacteria or renders them unable to replicate [3,6,10].

The presence of Ag^+ in B-550T/Ag and B-300S/Ag, confirmed by XPS, could be associated to the formation of Ag_2O or AgOH on the surface of metallic silver nanoparticles [37]; but also to the incorporation of Ag^+ by ionic exchange in the interlayer of the calcined sample (confirmed by XRD), or in the surface and edges in the clay particles of B-300S/Ag (since a decrement in Na^+ content was detected by EDXS).

The lower MIC for antibacterial activity obtained for the ground sample, is directly related to the higher ionic silver content, detected by XPS. If Ag^+ were concentrated only on the surface of the metallic silver nanoparticles, it would be expected that the ground sample showed the best results in both antibacterial tests. Nevertheless, the calcined sample, which contain a

lower proportion of Ag^+, presented a bigger inhibition zone in the disk susceptibility method, which suggest that the overall antibacterial effect is not only related to the presence and quantity of Ag^+ but also is affected by the surface characteristics of the samples, as reported by Zhao et al. [44].

In the disk method, the clays are pressed into pellets and deposited over the agar plate. The ground sample, present a lower pore size and a higher concentration of silver nanoparticles with a heterogeneous size distribution. It is probable that the bigger nanoparticles, 25–10 nm, as shown by SEM, agglomerate over the surface of the clay, clogging the pores and reducing the access of the bacteria to silver ions exchanged in the clay. Therefore, the antibacterial activity diminishes as was evidenced by a smaller inhibition zone. Similar results have been reported elsewhere when the disk method is used [4,37]. On the other hand, the use of clay powders in the minimum inhibitory concentration test, favors the interaction between the *E. coli* culture and the Ag^+ present in the clay.

4. Conclusions

Montmorillonite from Pellegrini Lake, Argentina, was treated by calcination and mechanical grinding and then subjected to cation exchange with silver. It was shown by X-ray diffraction and FTIR that the previous treatments affect the structure of the clays. Grinding causes the collapse of the interlayer structure and increase the specific surface area, whereas heating favors a phase transformation due to the loss of crystallization water. After silver modification, the formation of metallic silver nanoparticles over the clay aggregates was observed by SEM and HRTEM; nevertheless, the diminution on sodium content, evaluated by EDXS, and the displacement of (0 0 1) peak in B-550T/Ag suggest that silver was incorporated in the clay by ionic exchange. The silver modified clays showed good inhibition properties over the growth of *E. coli*, measured by the disk susceptibility and the MIC agar dilution tests; whereas the natural, calcined and ground samples did not showed any antibacterial activity. Antibacterial activity was attributed to the presence of ionic silver, confirmed by XPS. The silver modified ground sample presented the higher Ag^+ concentration and required the lower MIC to inhibit *E. coli* growth; although, the annealed sample showed a bigger inhibition zone in the disk susceptibility test. This behavior points out that the antibacterial performance is affected by the availability of the ionic silver to be in contact with the bacteria.

References

[1] B. Li, S. Yu, J.Y. Hwang, S. Shi, J. Miner. Mater. Charact. Eng. 1 (2002) 61–68.
[2] F. Ohashi, A. Oya, L. Duclaux, F. Beguin, Appl. Clay Sci. 12 (1998) 435–445.
[3] D. Zhao, J. Zhou, N. Liu, Appl. Clay Sci. 33 (2006) 161–170.
[4] A. Top, S. Ulku, Appl. Clay Sci. 27 (2004) 13–19.
[5] M. Rivera-Garza, M.T. Olguín, I. García-Sosa, D. Alcántara, G. Rodríguez-Fuentes, Micropor. Mesopor. Mater. 39 (2000) 431–444.
[6] B. Dizman, J.C. Badger, M.O. Elasri, L.J. Mathias, Appl. Clay Sci. 38 (2007) 57–63.
[7] M.I. Carretero, Appl. Clay Sci. 21 (2002) 155–163.
[8] D.M. Moore, R.C. Reynolds, X-ray Diffraction and the Identification and Analysis of Clay Minerals, second ed., Oxford University Press, New York, 1997.
[9] C. Viseras, C. Aguzzi, P. Cerezo, A. Lopez-Galindo, Appl. Clay Sci. 36 (2007) 37–50.
[10] C.-H. Hu, M.-S. Xia, Appl. Clay Sci. 31 (2006) 180–184.
[11] B. Lombardi, M. Baschini, R.M. Torres Sánchez, Appl. Clay Sci. 24 (2003) 43–50.
[12] M. Damonte, R.M. Torres Sánchez, M. dos Santos Afonso, Appl. Clay Sci. 36 (2007) 86–94.
[13] J.W. Jaynes, R. Zartman, W. Hudnall, Appl. Clay Sci. 36 (2007) 197–205.
[14] F. Bonina, M. Giannossi, L. Medici, C. Puglia, V. Summa, F. Tateo, Appl. Clay Sci. 36 (2007) 77–85.
[15] E. Bojemueller, A. Nennemann, G. Lagaly, Appl. Clay Sci. 18 (2001) 277–284.
[16] C. Volzone, L.B. Garrido, CERÂMICA 47 (2001) 4–8.
[17] C. Aguzzi, P. Cerezo, C. Viseras, C. Caramella, Appl. Clay Sci. 36 (2007) 22–36.
[18] R.M. Torres Sánchez, Colloid Surf. A 127 (1997) 135–140.
[19] B. Lombardi, M. Baschini, R.M. Torres Sanchez, Appl. Clay Sci. 22 (2003) 309–312.
[20] R.M. Torres Sánchez, M. Genet, S. Yunes. XV Cong. AFQQI. C-95 Tandil, 2007.
[21] National Committee for Clinical Laboratory Standards. Performance standards of antimicrobial disk susceptibility test. Approved Standard M02-A8. Wayne, PA: NCCLS, 2000.
[22] J. Hindler, in: Henry D.I. Semberg (Ed.), Clinical Microbiology Procedures Handbook, American Society for Microbiology, Washington, DC, USA, 2004.
[23] R. Armisen, F. Galatas, in: G. Phillips, P. Williams (Eds.), Handbook of Hydrocolloids, Woodhead Publishing, Cambridge, UK, 2000.
[24] R.M. Torres Sánchez, V. Lastiri, in: R. Trindade, R. Melamed, L. Gonzaga, S. Sobrado, J. Peres Barbosa (Eds.), XIII International Conference on Heavy metals in the environment, Rio de Janeiro, 2005, CD. ISBN 85-7227-212-7.
[25] R.V. Gaines, H.C.W. Skinner, E.E. Foord, B. Mason, A. Rosenzweig, Dana's New Mineralogy, eighth ed., John Wiley & Sons, New York, 1997.
[26] C. Volzone, L.B. Garrido, Clay Miner. 36 (2001) 115–123.
[27] S. Aceman, N. Lahav, S. Yariv, Appl. Clay Sci. 17 (2000) 99–126.
[28] I. Sondi, M. Stubicar, V. Pravdic, Colloids Surf. A: Physicochem. Eng. Aspects 127 (1997) 141–149.
[29] J. Liu, X. Li, S. Zuo, Y. Yu, Appl. Clay Sci. 37 (2007) 275–280.
[30] A. Chatterjee, J. Chem. Sci. 117 (2005) 533–539.
[31] F. Secundo, J. Miehé-Brendlé, C. Chelaru, E.E. Ferrandi, E. Dumitriu, Micropor. Mesopor. Mater. 109 (2008) 350–361.
[32] J.T. Kloprogge, E. Mahmutagic, R.L. Frost, J. Colloid Interface Sci. 296 (2006) 640–646.
[33] A. Bakhti, Z. Derriche, A. Iddou, M. Larid, Eur. J. Soil Sci. 52 (2001) 683–692.
[34] I. De la Rosa-Gómez, M.T. Olguín, D. Alcántara, J. Environ. Manage. (2007) doi:10.1016/j.jenvman.2007.04.005.
[35] Y. Inoue, Y. Kanzaki, J. Inorg. Biochem. 67 (1997) 1–4.
[36] S.S. Djokic, R.E. Burrell, J. Electrochem. Soc. 145 (1998) 1426–1430.
[37] H. Ortiz-Ibarra, N. Casillas, V. Soto, M. Barcena-Soto, R. Torres-Vitela, W. de la Cruz, S. Gómez-Salazar, J. Colloid Interface Sci. 314 (2007) 562–571.
[38] F.-R.F. Fan, A.J. Bard, J. Phys. Chem. B 106 (2002) 279–287.
[39] XPS and Auger Handbook. Thermo VG-Scientific. Doc. Number: 600001 issue 2, 2003.
[40] X. Tang, J. Chen, Y. Li, Y. Li, Y. Xu, W. Shen, Chem. Eng. J. 118 (2006) 119–125.
[41] K.S.W. Sing, D.H. Everett, R.A.W. Haul, L. Moscou, R.A. Pierotti, J. Rouquérol, T. Siemieniewska, Pure Appl. Chem. 57 (1985) 603–619.
[42] M. Kruk, M. Jaroniec, Chem. Mater. 13 (2001) 3169–3183.
[43] C. Volzone, J.G. Thompson, A. Melnitchenko, J. Ortiga, S.R. Palethorpe, Clays Clay Miner. 47 (1999) 647–657.
[44] J. Zhao, H.J. Feng, H.Q. Tang, J.H. Zheng, Surf. Coat. Technol. 201 (2007) 5676–5679.